Published in final edited form as:

Nat Genet. 2009 September ; 41(9): 1032–1036. doi:10.1038/ng.423.

Mutations in the *inositol polyphosphate-5-phosphatase E* gene link phosphatidyl inositol signaling to the ciliopathies

Stephanie L. Bielas[1,*], **Jennifer L. Silhavy**[1,*], **Francesco Brancati**[2,3,*], **Marina V. Kisseleva**[4,*], **Lihadh Al-Gazali**[5,*], **Laszlo Sztriha**[6], **Riad A. Bayoumi**[7], **Maha S. Zaki**[8], **Alice Abdel-Aleem**[9], **Ozgur Rosti**[10], **Hulya Kayserili**[10], **Dominika Swistun**[1], **Lesley C. Scott**[1], **Enrico Bertini**[11], **Eugen Boltshauser**[12], **Elisa Fazzi**[13], **Lorena Travaglini**[2], **Seth J. Field**[14], **Stephanie Gayral**[15], **Monique Jacoby**[15], **Stephane Schurmans**[15], **Bruno Dallapiccola**[2,16], **Philip W. Majerus**[4], **Enza Maria Valente**[2,17], and **Joseph G. Gleeson**[1]

[1]Neurogenetics Laboratory, Howard Hughes Medical Institute, Department of Neurosciences and Pediatrics, University of California, San Diego, USA, 92093. [2]CSS-Mendel Institute, Casa Sollievo della Sofferenza Hospital, viale Regina Margherita 261, 00198 Rome, Italy. [3]Department of Biomedical Sciences and Aging Research Center, Ce.S.I., G. d'Annunzio University Foundation, Chieti, Italy. [4]Divisionof Hematology, Department of Internal Medicine, Washington University School of Medicine, St. Louis, Missouri, USA, 63132. [5]Departments of Pediatrics and Pathology, United Arab Emirates University, Faculty of Medicine and Health Sciences, PO Box 17616, Al Ain, UAE. [6]Department of Pediatrics, University of Szeged, Temesvárikrt. 35-37, Szeged H-6726, Hungary. [7]College of Medicine, Sultan Qaboos University, P.O. Box 35, Al-Khoud 123, Sultanate of Oman. [8]Clinical Genetics Department, Human Genetics and Genome Research Division, National Research Centre, El-Tahrir Street, Dokki, Cairo, Egypt. [9]Medical Molecular Genetics Department, Human Genetics and Genome Research Division, National Research Centre, El-Tahrir Street, Dokki, Cairo, Egypt. [10]Istanbul University, Istanbul Medical Faculty, Medical Genetics, Millet Caddesi, Capa, Fatih, 034104 Istanbul, Turkey. [11]Unit of Molecular Medicine, Department of Laboratory Medicine, Bambino Gesu Children's Research Hospital, P.za S. Onofrio, 4, 00165, Rome, Italy. [12]Department of Paediatric Neurology, University Children's Hospital of Zurich, Steinwiesstrasse 75, CH-8032, Zurich, Switzerland. [13]Department of Child Neurology and Psychiatry, IRCCS C. Mondino Institute of Neurology, Via Mondino 2, 27100, Pavia, Italy. [14]Division of Endocrinology and Metabolism, Department of Medicine, University of California, San Diego, USA, 92093. [15]IRIBHM, Université Libre de Bruxelles, Gosselies, Belgium [16]Department of Experimental Medicine, Sapienza University, Rome, Italy. [17]Department of Medical and Surgical Paediatric Sciences, University of Messina, Messina, Italy.

Correspondence should be addressed to J.G.G (jogleeson@ucsd.edu)..

Author Contributions S.L.B, J.L.S, F.B., L.C.S., L.T., S.G., M.J., S.S., M.K. performed experiments, L.A-G., L.S. M.S.Z, A.A-A, O.R., H.K., D.S., L.C.S., E.B., E.B., E.F. identified and recruited patients, R.A.B. shared unpublished data and reagents, S.J.F., B.D., P.W.M. provided advice and helped with data interpretation, S.L.B and J.L.S assembled the figures, S.L.B, E.M.V. and J.G.G. wrote and edited the manuscript.

*These authors contributed equally to this work.

GenBank accession numbers. Human *INPP5E* is assigned GenBank number NM_019892, and the encoded protein NP_063945. There is one minor splice variant annotated in human (U45974), due to a deletion of the 3′ stop codon, resulting in an additional 50 amino acids of the C-terminal protein. This stretch has no similarity in the database and is of unknown function.

Abstract

Phosphotidylinositol (PtdIns) signaling is tightly regulated, both spatially and temporally, by subcellularly localized PtdIns kinases and phosphatases that dynamically alter downstream signaling events 1. Joubert Syndrome (JS) characterized by a specific midbrain-hindbrain malformation ("molar tooth sign") and variably associated retinal dystrophy, nephronophthisis, liver fibrosis and polydactyly 2, and is included in the newly emerging group of "ciliopathies". In patients linking to *JBTS1*, we identified mutations in the *INPP5E* gene, encoding *inositol polyphosphate-5-phosphatase E*, which hydrolyzes the 5-phosphate of PtdIns(3,4,5)P3 and PtdIns(4,5)P2. Mutations clustered in the phosphatase domain and impaired 5-phosphatase activity, resulting in altered cellular PtdIns ratios. INPP5E localized to cilia in major organs affected in JS, and mutations promoted premature destabilization of cilia in response to stimulation. Thus, these data links PtdIns signaling to the primary cilium, a cellular structure that is becoming increasingly appreciated for its role in mediating cell signals and neuronal function.

Joubert syndrome locus 1 (*JBTS1*, MIM%213300) was mapped to the distal q-arm of chromosome 9, between D9S1826-D9S1838 3, in two JS Emirate families variably associated with retinopathy, and a proven "molar tooth" sign (MTI-007 and MTI-008 previously called Family A and C, respectively, Fig. 1a, Supplemental Table 1) 3. To refine the candidate interval, we recruited two additional unaffected MTI-007 and two affected MTI-008 family members, and performed a 5K SNP analysis, confirming *JBTS1* in MTI-007 (Supplemental Fig. 1). Family MTI-008 produced a linkage peak at *JBTS1*, among several other peaks of similar amplitude, with a maximum LOD score of about +1.94. As a result, these SNP scans failed to significantly narrow the candidate interval (Supplemental Table 2).

An additional 25 consanguineous families with JS were analyzed, and three (MTI-134, MTI-610, and MTI-627, of Emirate, Turkish and Egyptian descent) showed at least one peak that overlapped with *JBTS1*. Two Italian families (COR-10 and COR-21) also linked to *JBTS1* 4. Haplotype analysis suggested that MTI-007 and MTI-134 were identical-by-descent, as were COR-10 and COR-21 (data not shown). Together these analyses defined a candidate interval of 3.5 MB in distal 9q34.2-tel, containing approximately 86 annotated candidate genes (Supplemental Table 3), 57 of which were screened for sequence changes, whereas the remaining 29 either lacked an open reading frame or were excluded due to lack of developmental expression. This extensive screening identified the *INPP5E* gene as mutated in each *JBTS1*-linked family (Fig. 1a-b).

The *INPP5E* mutations were notable for two reasons. First, all identified mutations were amino acid transversions that clustered within the enzymatically-active phosphatase domain (Fig. 1b). Second, each altered the charge of highly basic evolutionarily conserved amino acid residues (Fig. 1c), together suggesting that these mutations might alter enzymatic activity. None of these mutations were encountered among 188 control chromosomes from healthy ethnically matched individuals, and all segregated with the disease in each family. We modeled these mutations using the published crystal structure of synaptojanin5, the only inositol 5-phosphatase for which structural data is available. We found that each of the altered residues (with one exception, R563) was predicted to project its charged tail toward

the presumed binding pocket of the PtdIns substrate (Supplemental Fig. 2), suggesting that these mutations might alter substrate specificity.

To test the effects of INPP5E mutations on PtdIns phosphatase activity, we immunoprecipated tagged wildtype and enzymatically null (D477N 6), together with each mutation separately from mammalian cells (resulting in similar protein levels, Supplemental Fig. 3) and then analyzed phosphatase activity against PtdIns(3,4,5)P3 and PtdIns(4,5)P2, the presumed cellular INPP5E substrates (Fig. 2a). We found that each of the *JBTS1* missense mutations severely disrupted phosphatase activity towards PtdIns(3,4,5)P3 (Fig. 2b, $p < 0.05$ activity for each mutant, N = 3 independent experiments). Of note, since the R512W/R515W variants were observed on a single haplotype, we reasoned that probably only one was driving the defect in enzymatic activity, and under separate analysis, the R515W mutation was shown to be the major contributor to the defective enzymatic activity (data not shown). Comparison with phosphatase activity using PtdIns(4,5)P2 as substrate showed similar although not as severely compromised results as compared with wildtype (Fig. 2c), suggesting that PtdIns(3,4,5)P3 may be the relevant substrate in *JBTS1*. Because overexpression of INPP5E was previously shown to block Akt phosphorylation in response to PDGF stimulation in cultured cells (presumably by depleting levels of PtdIns(3,4,5)P3 and PtdIns(4,5)P2) 7, we next tested the effect of overexpression of each of the patient mutations in this published assay. Not only did patient mutations fail to block Akt signaling, but elevated basal levels of pAkt were also apparent in unstimulated cells (Supplemental Fig. 4). We conclude that the *JBTS1*-associated missense mutations impair phosphatase activity towards putative PtdIns substrates, which can alter downstream signaling events.

Next, we tested whether the absence of endogenous catalytic INPP5E activity results in an altered PtdIns profiles in cells. Although difficult to measure absolute levels PtdIns moieties in cells, the model predicted an increased ratio of PtdIns(4,5)P2/PtdIns(4)P due to a block in this enzymatic step (Fig. 2a), and thus skin fibroblasts from MTI-610 patient 1 and 2 (brother and sister) were assessed for PtdIns(4,5)P2/PtdIns(4)P ratio. In control unstimulated growth-arrested fibroblasts we found a PtdIns(4,5)P2/PtdIns(4)P ratio of about 0.63, whereas in both patient fibroblast samples the ratio was increased by about 20% ($p = 0.05$, N = 3 independent experiments, Fig. 2c). We found no differences in expression levels of INPP5E in this or other patient fibroblast samples with *INPP5E* mutations (Supplemental Fig. 5). We conclude that catalytic activity of INPP5E is required for maintenance of homeostatic ratios of PtdIns in cells.

In order to investigate a possible connection with ciliopathies, we examined INPP5E localization in cells with well-described cilia. The RPE-hTERT line (immortalized retinal pigment epithelia) display a primary cilia in >80% of growth-arrested cells 8,9. Coimmunostaining with pericentrin, a marker of the pericentriolar matrix, showed INPP5E immediately adjacent to the base of the cilium (Fig. 3a). This was confirmed by INPP5E coimmunostaining with acetylated tubulin, a marker of the ciliary axoneme, as well as with ARL13B, a cilia marker 10-12, which showed tight-colocalization of INPP5E to the ciliary axoneme, with only minimal INPP5E localized to non-ciliary locations (Fig. 3b). Transfection of wild-type GFP-tagged INPP5E into IMCD-3 cells under ciliary-permissive conditions demonstrated ciliary localization (Supplemental Fig. 6), and we found no defect

in ciliary localization of any of the *JBTS1*-associated patient missense mutations when expressed in these cells (data not shown). By contrast, cells at mitotic stages (after cilium withdrawal) showed cytoplasmic localization (Supplemental Fig. 7). The data suggests that INPP5E localizes predominantly to the primary cilium during interphase in the cell lines tested.

We stained for INPP5E in organs affected in JS from the GFP-Centrin2 transgenic mouse (marks the base of the cilium) 13, and identified cilia localization in each. In renal collecting tubules, cilia were evident projecting from the epithelium into the lumen. In this mouse, many cells were marked by luminal localization of the pair of centrioles, and from this site, the majority of cells had an INPP5E-positive cilium projecting into the lumen (Fig. 3c). In the developing cerebellum, cilia have been identified on a population of neuroblasts in the cerebellar internal granule layer 14. We identified these ciliated cells based upon GFP signal at the centrioles, and identified INPP5E-positive cilia projecting into the parenchyma in the vast majority of these cells (Fig. 3d), and similar ciliary localization was observed in the hepatic bile ducts (not shown). We also observed that INPP5E localized to the region adjacent to the basal body and connecting cilium in retinal photoreceptor cells (Fig. 3e-f). Therefore, INPP5E is predominantly localized adjacent to or within the cilium in each of the major organs affected in JS.

To assess the potential function of INPP5E at the primary cilium, we utilized primary fibroblasts from patient MTI-610-V-1. These cells displayed essentially normal growth characteristics, as well as percentage of ciliated cells compared with controls (81% vs. 76%, $p > 0.05$, Fig. 4a), suggesting that *INPP5E* enzymatic activity is not required for ciliogenesis or cilia maintenance, at least not in fibroblasts. However, the cilium is not a fixed structure, and is labile to the application of serum-derived factors such as PDGF 15. Since serum is a potent activator of the PtdIns pathway in cultured cells, we predicted that the altered PtdIns profile might render cilia in mutant cells more labile to the application of serum. We applied serum to control and MTI-610-V-1 cells and scored the percentage of cells retaining a cilium, based upon acetylated-tubulin and ARL13B staining at specific time intervals. By 4 hr after serum application, wild-type cells had an 8% cilia withdrawal rate whereas *INPP5E* mutant cells had a 33% cilia withdrawal rate, (73% vs. 43%, $p < 0.01$, N = 3 independent experiments). At the 8 hr and 24 hr timepoints, the percentage of cells with visible cilia had equalized to about 40% in the two genotypes, suggesting that *INPP5E* controls timing of cilia disassembly during early response to serum.

To determine if the reduced number of ciliated mutant cells is due to an enhanced rate of cilia withdrawal in the absence of functional INPP5E, we performed scanning electron microscopy. Prior to the addition of serum, we found that the length of the primary cilium was approximately the same in control vs. MTI-610-V-1 serum-starved fibroblasts, measuring ~3 um in length (Fig. 4b-e). At the 4 hr timepoint (where we saw the maximal difference in cilia number), however, cilium length of the MTI-610 fibroblasts was about half of control. These data were quantified in *x-y* sections from cells with remaining visible cilia as evidenced by immunostaining for ARL13B prior to, and then at 4 hr and 8 hr after serum addition. We found a significant decrease in average cilia length at 4 hr after serum stimulation in mutant vs. controls (2.73 vs. 1.28 um, wildtype vs. MTI-610, $p < 0.01$, $n > 30$

cells for each condition), whereas no difference was apparent either before serum or after 8 hrs (Supplemental Fig. 8). Thus ciliary disassembly is more rapid in the absence of full INPP5E activity compared with wildtype.

Following ascertainment of fibroblast samples from additional patients with *INPP5E* mutations, we noted some alterations in cell proliferation rates in culture, and thus tested quiescent cells for ability to reenter the cell cycle. While MTI-610 fibroblasts had no apparent alteration in cell cycle reentry (based upon Ki67 staining or BrdU incorporation), MTI-134 and MTI-627 exhibited a reduction in the percentage of mitotically active cells following serum addition (Supplemental Fig. 9). As MTI-134 and MTI-627 had more severe reduction in enzymatic activity than MTI-610 in the *in vitro* assay (0% and 8.5% vs.15%, presented in Fig. 2), the data suggests that residual but not full function of INPP5E may be required for this serum-based cell-cycle reentry. MTI-610 fibroblasts exhibited a normal percentage of mitotically active cells, however, a greater percentage of these mitotically synchronized cells reentered the cell cycle initially (Ki67 staining between 18-24hrs) and progressed through the cell cycle more rapidly (reduction of BduU incorporation from 24hrs to 30hrs) than control fibroblasts, suggesting that INPP5E enzymatic activity may also influence the rate of cell cycle progression. Not all serum-based responses are abnormal in these patient samples, however. For instance, there were no alterations in low-dose serum-dependent scratch-wound assay healing (Supplemental Fig. 10), which we designed to be migration-dependent but largely proliferation-independent 16. We conclude that INPP5E may play specific serum-dependent cellular roles, mediating both ciliary stability as well as cell cycle dynamics.

Our data demonstrates that hypomorphic mutations in *INPP5E* lead to JS, providing the first evidence of a link between PtdIns signaling and the ciliopathies. It will be important to determine if the developmental defects observed in JS are the result of defects in cilia maintenance or due to a more broadly defined disruption in PtdIns signaling. Since PDGFαα receptor has been localized to primary cilia 17, and since PDGF is one of the key serum-derived factors that mediates cilia withdrawal concurrent with cell cycle reentry 18 it is possible that PDGF and other factors that utilize cilia as signaling centers have downstream pathways that are regulated through specific localization and function of INPP5E.

Previous studies have hinted at possible connections between PtdIns signaling and the cilium. Tubby mutant mice have cilia-like phenotypes and the protein encoded from the mutant gene binds specific PtdIns including PtdIns3,4,5(P3) 19. Furthermore, Bardet-Biedl syndrome shares similar ciliopathy features to JS, and the BBS5 protein can bind PtdIns 9. However, our findings are the first, to our knowledge, to directly implicate defective enzymatic conversion within the PtdIns class. The fact that INPP5E displays enrichment within the ciliary axoneme makes it tempting to speculate that PtdIns signaling may not just function to regulate cilia stability, but also that this signaling may occur *within* the cilium. An alternative model is that INPP5E might be sequestered within the cilium, but exert its activity within the cytoplasm, similar to the models being proposed for Sonic hedgehog signaling 20. The identification of a key regulatory enzyme in this process highlights an important area of research with clinical relevance.

Methods

Patients and families

Twenty-seven consanguineous families from the Middle East, Turkey and Europe were included in this study based upon the following criteria: 1) at least one individual with a neuroradiographically proven “molar tooth sign” associated with any JS or related disorder phenotype; 2) evidence for linkage to the *JBTS1* locus; 3) exclusion of linkage to any other of the known JBTS loci (*JBTS2-9*). Whenever possible, patients underwent a full diagnostic protocol as previously reported 21. Brain MRI analysis was completed during the clinical assessment using standard sequence protocols. Parental written informed consent was obtained from all families, and the study was approved by the HRPP Committees of UCSD (La Jolla) and CSS-Mendel Institute (Rome).

Genome-wide screen and fine mapping of the *JBTS1* locus

A 5K whole genome linkage scan was performed in all informative families using the Illumina Linkage IVb mapping panel 22, and analyzed with easyLINKAGE-Plus software 23, which runs Allegro version 1.2c in a PC Windows interface to calculate multipoint LOD scores. Parameters were set to autosomal recessive with full penetrance, and disease allele frequency of 0.001. Fine mapping on selected individuals was performed with the Affymetrix 250K Nsp1 SNP array and results analyzed using pedigree-free identity-by-descent mapping. Short tandem repeat polymorphic markers at the *JBTS1* locus were used as previously published 4.

Mutation screening

Mutations were screened using a combination of single stranded conformational polymorphism analysis and direct sequencing as described 24,25.

Bioinformatics

Protein evolutionary conservation was determined by aligning amino acids from the Human Genome Browser (http://www.genome.ucsc.edu). Ciliary proteome was searched using web-based tools 26,27. Protein folding and intermolecular interactions were predicted using Swiss-Model with crystallized PtdIns 5-phosphatase domain of synaptojanin bound to Ca(2+) and PtdIns(1,4)P2 5. The resulting INPP5E structure was manipulated with PyMOL software by importing amino acid sequence for wildtype and mutant and comparing the likely docking site for PtdIns.

Biochemical assays

INPP5E cDNA 7 was cloned in frame with EGFP into pcDNA3.0 for expression. Patient mutations were individually engineered into the *INPP5E* cDNA in a Myc-tagged vector, stably transfected into 293T cells using the T-Rex tetracycline-regulated system (Invitogen)7, immunoprecipitated using Myc-tag, confirmed by Western to each express comparable amounts (Supplemental Fig. 3), and then used in a modified PtdIns(4,5)P2 hydrolysis assay as described 28. PtdIns(3,4,5)P3 hydrolysis was measured by adding purified substrate to the immunoprecipitates at 37°C for 10 min, followed by malachite

green for an additional 10 min 29. Released inorganic phosphate was measured at 650 nm, compared against a standard curve, and performed in triplicate. Assessment of PtdIns(4,5)P2/PtdIns(4)P ratio from patient primary cells were metabolically labeled and performed as described 30. Stably transfected 293T cells were stimulated with 50ng/ml of PDGF and analyzed for Akt signaling as described7.

Histology

Mouse tissues from wildtype or GFP-CETN2 mice were immunostained with an affinity purified peptide-specific INPP5E rabbit antisera that reacts with human and mouse as reported 31 at 1:200 and images acquired on a DeltaVision imaging system with 5-10 cycles of deconvolution.

Fibroblasts assay

Primary skin fibroblasts from patient and unaffected passage-matched control were grown at similar confluence for 3 days in the absence of serum. Ciliary disassembly and wound healing was assessed as described 18,32. Cell-cycle re-entry was interrogated as described 33 with 20% serum addition to sub-confluent fibroblasts. BrdU (10 uM) was applied for 1 hr, and antigens detected with antibodies to Ki67(1:1000) and BrdU (1:1500) (Abcam # ab66155 and ab6326).

Scanning Electron microscopy

Fibroblasts were fixed in 2.5% glutaraldehyde/0.1 M cacodylate buffer (CB) (pH 7.4) for 30 min at 25C, rinsed (0.1 M CB), postfixed (1% OsO4/0.1 M CB) for 30 min at 4C, dehydrated with a graded alcohol series, which was displaced with hexamethyldisilazane, and evaporated overnight before sputter coating samples with palladium and imaged on XL30 ESEM-FEG.

Cilia length quantification

Cilia length was correlated in the *x*-*y*-*z* vs. *x*-*y* using the Volocity rendering software. 3D reconstruction of cilia using DeltaVision imaging system with 100X objective with 0.1 um *z*-steps allowed for length assessment irrespective of angle of orientation. Cilia length was also measured in the same cells using *x*-*y* only projections, and measurements were compared for five cells. No observable difference in cilia length measurements were detected, and thus subsequent lengths were measured from *x*-*y* projections.

Supplementary Material

Refer to Web version on PubMed Central for supplementary material.

Acknowledgements

We thank the Marshfield Clinic Research Foundation, Center for Inherited Disease Research and UCLA Microarray Core (supported by NHBLI and NIH) for genotyping support. Jennifer Meerloo at the UCSD Neuroscience Microscopy Imaging Core provided imaging support. Ryan Anderson of the UCSD Material Sciences provided electron microscopy support. We thank the Dixon lab (UCSD) for suggestions and help with protein modeling, the Mitchell lab (Monash University) for reagents, and the Schumans lab (IBMM) for help with the phosphatase assay and for communicating results prior to publication. This work was supported by the UCSD

Neuroplasticity of Aging Training Grant (to SLB.), Italian Ministry of Health (RC2008 to BD, Ricerca Finalizzata 2006 to EMV), Telethon Foundation Italy (GGP08145 to EB/EMV) NIH HL 16634 (PWM and MVK), American Heart Association Grant 0730350N (MVK), NINDS, Burroughs Welcome Fund, the March of Dimes, and the Howard Hughes Medical Institute (to JGG).

References

1. Vicinanza M, D'Angelo G, Di Campli A, De Matteis MA. Phosphoinositides as regulators of membrane trafficking in health and disease. Cell Mol Life Sci. 2008
2. Valente EM, Brancati F, Dallapiccola B. Genotypes and phenotypes of Joubert syndrome and related disorders. Eur J Med Genet. 2008; 51:1–23. [PubMed: 18164675]
3. Saar K, et al. Homozygosity mapping in families with Joubert syndrome identifies a locus on chromosome 9q34.3 and evidence for genetic heterogeneity. Am J Hum Genet. 1999; 65:1666–71. [PubMed: 10577920]
4. Valente EM, et al. Distinguishing the four genetic causes of Joubert syndrome-related disorders. Ann Neurol. 2005; 57:513–9. [PubMed: 15786477]
5. Tsujishita Y, Guo S, Stolz LE, York JD, Hurley JH. Specificity determinants in phosphoinositide dephosphorylation: crystal structure of an archetypal inositol polyphosphate 5-phosphatase. Cell. 2001; 105:379–89. [PubMed: 11348594]
6. Kong AM, et al. Phosphatidylinositol 3-phosphate [PtdIns3P] is generated at the plasma membrane by an inositol polyphosphate 5-phosphatase: endogenous PtdIns3P can promote GLUT4 translocation to the plasma membrane. Mol Cell Biol. 2006; 26:6065–81. [PubMed: 16880518]
7. Kisseleva MV, Cao L, Majerus PW. Phosphoinositide-specific inositol polyphosphate 5-phosphatase IV inhibits Akt/protein kinase B phosphorylation and leads to apoptotic cell death. J Biol Chem. 2002; 277:6266–72. [PubMed: 11706019]
8. Jiang XR, et al. Telomerase expression in human somatic cells does not induce changes associated with a transformed phenotype. Nat Genet. 1999; 21:111–4. [PubMed: 9916802]
9. Nachury MV, et al. A core complex of BBS proteins cooperates with the GTPase Rab8 to promote ciliary membrane biogenesis. Cell. 2007; 129:1201–13. [PubMed: 17574030]
10. Cantagrel V, et al. Mutations in the cilia gene ARL13B lead to the classical form of Joubert syndrome. Am J Hum Genet. 2008; 83:170–9. [PubMed: 18674751]
11. Caspary T, Larkins CE, Anderson KV. The graded response to Sonic Hedgehog depends on cilia architecture. Dev Cell. 2007; 12:767–78. [PubMed: 17488627]
12. Alieva IB, Gorgidze LA, Komarova YA, Chernobelskaya OA, Vorobjev IA. Experimental model for studying the primary cilia in tissue culture cells. Membr Cell Biol. 1999; 12:895–905. [PubMed: 10512057]
13. Higginbotham H, Bielas S, Tanaka T, Gleeson JG. Transgenic mouse line with green-fluorescent protein-labeled Centrin 2 allows visualization of the centrosome in living cells. Transgenic Res. 2004; 13:155–64. [PubMed: 15198203]
14. Chizhikov VV, et al. Cilia proteins control cerebellar morphogenesis by promoting expansion of the granule progenitor pool. J Neurosci. 2007; 27:9780–9. [PubMed: 17804638]
15. Tucker RW, Pardee AB, Fujiwara K. Centriole ciliation is related to quiescence and DNA synthesis in 3T3 cells. Cell. 1979; 17:527–35. [PubMed: 476831]
16. De Donatis A, et al. Proliferation versus migration in platelet-derived growth factor signaling: the key role of endocytosis. J Biol Chem. 2008; 283:19948–56. [PubMed: 18499659]
17. Schneider L, et al. PDGFRalphaalpha signaling is regulated through the primary cilium in fibroblasts. Curr Biol. 2005; 15:1861–6. [PubMed: 16243034]
18. Pugacheva EN, Jablonski SA, Hartman TR, Henske EP, Golemis EA. HEF1-dependent Aurora A activation induces disassembly of the primary cilium. Cell. 2007; 129:1351–63. [PubMed: 17604723]
19. Santagata S, et al. G-protein signaling through tubby proteins. Science. 2001; 292:2041–50. [PubMed: 11375483]
20. Rohatgi R, Scott MP. Arrestin' Movement in Cilia. Science. 2008; 320:1726–7. [PubMed: 18583599]

21. Valente EM, et al. AHI1 gene mutations cause specific forms of Joubert syndrome-related disorders. Ann Neurol. 2006; 59:527–534. [PubMed: 16453322]
22. Murray SS, et al. A highly informative SNP linkage panel for human genetic studies. Nat Methods. 2004; 1:113–7. [PubMed: 15782173]
23. Hoffmann K, Lindner TH. easyLINKAGE-Plus--automated linkage analyses using large-scale SNP data. Bioinformatics. 2005; 21:3565–7. [PubMed: 16014370]
24. Gleeson JG, et al. Genetic and neuroradiological heterogeneity of double cortex syndrome. Ann Neurol. 2000; 47:265–9. [PubMed: 10665503]
25. Valente EM, et al. Mutations in CEP290, which encodes a centrosomal protein, cause pleiotropic forms of Joubert syndrome. Nat Genet. 2006; 38:623–5. [PubMed: 16682970]
26. Inglis PN, Boroevich KA, Leroux MR. Piecing together a ciliome. Trends Genet. 2006; 22:491–500. [PubMed: 16860433]
27. Gherman A, Davis EE, Katsanis N. The ciliary proteome database: an integrated community resource for the genetic and functional dissection of cilia. Nat Genet. 2006; 38:961–2. [PubMed: 16940995]
28. Caldwell KK, Lips DL, Bansal VS, Majerus PW. Isolation and characterization of two 3-phosphatases that hydrolyze both phosphatidylinositol 3-phosphate and inositol 1,3-bisphosphate. J Biol Chem. 1991; 266:18378–86. [PubMed: 1655747]
29. Vandeput F, Backers K, Villeret V, Pesesse X, Erneux C. The influence of anionic lipids on SHIP2 phosphatidylinositol 3,4,5-trisphosphate 5-phosphatase activity. Cell Signal. 2006; 18:2193–9. [PubMed: 16824732]
30. Zhang X, Hartz PA, Philip E, Racusen LC, Majerus PW. Cell lines from kidney proximal tubules of a patient with Lowe syndrome lack OCRL inositol polyphosphate 5-phosphatase and accumulate phosphatidylinositol 4,5-bisphosphate. J Biol Chem. 1998; 273:1574–82. [PubMed: 9430698]
31. Kisseleva MV, Wilson MP, Majerus PW. The isolation and characterization of a cDNA encoding phospholipid-specific inositol polyphosphate 5-phosphatase. J Biol Chem. 2000; 275:20110–6. [PubMed: 10764818]
32. Rodriguez LG, Wu X, Guan JL. Wound-healing assay. Methods Mol Biol. 2005; 294:23–9. [PubMed: 15576902]
33. Kim J, Krishnaswami SR, Gleeson JG. CEP290 interacts with the centriolar satellite component PCM-1 and is required for Rab8 localization to the primary cilium. Hum Mol Genet. 2008; 17:3796–805. [PubMed: 18772192]

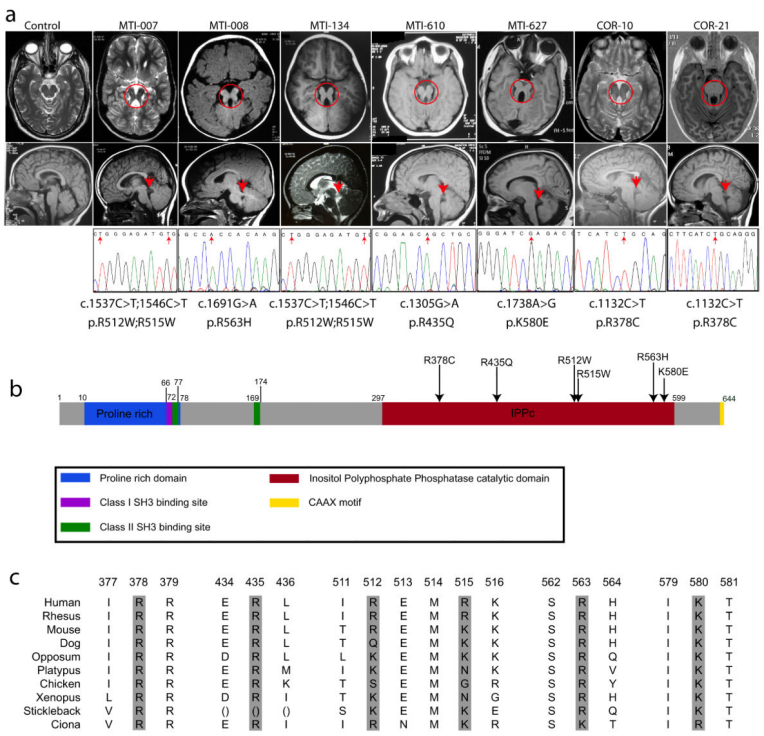

Figure 1.

Missense mutations in the encoded enzymatic domain of *INPP5E*, (inositol polyphate-5-phosphatase E) in patients linked to the *JBTS1* locus. **(a)** Top: axial brain MRIs showing molar tooth sign (red circle) from one affected from each linked family, representing four different countries of origin. Bottom: midline sagittal MRIs showing horizontally-oriented superior cerebellar peduncle (red arrow), not evident in control. Sequence chromatograms from one affected from each family, showing the nucleotide change (red arrow), with corresponding amino acid substitution listed below. Families MTI-007 and MTI-134 shared a common haplotype at the *JBTS1* locus, as did COR-10 and COR-21, and they share common mutations. MTI-007 and MTI-134 have a compound homozygous mutation with a double R512W; R515W. **(b)** Predicted protein domains of INPP5E indicated by color. Each of the identified missense mutations (arrows) occurs in a basic residue within the catalytic domain and alters charge. **(c)** Evolutionary conservation of mutated amino acids.

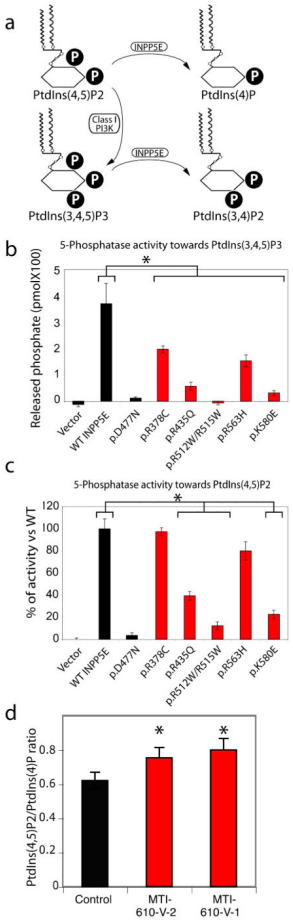

Figure 2.

Impaired 5-phosphatase activity and altered ratio of PtdIns(4,5)P2 to PtdIns(4)P associated with *JBTS1 INPP5E* mutations. **(a)** Summary of PtdIns metabolism. P = phosphate. A block in INPP5E function is predicted to increase the PtdIns(4,5)P2:PtdIns(4)P ratio. **(b-c)** More severe reduction in 5-phosphatase activity of mutant INPP5E against PtdIns(3,4,5)P3 than PtdIns(4,5)P2 substrates. Note that activity was largely retained against PtdIns(4,5)2 for some mutations (mutants R435Q, R512W/R515W and K580E are severely defective, whereas R378C and R563H are only slightly diminished). D477N is known phosphatasedead, compared with each of the patient mutations. (N = 3 for each sample) **(d)** Elevated ratio of PtdIns(4,5)P2 to PtdIns(4)P in patient primary fibroblast lines MTI-610-V-2 and V-1, compared with control fibroblast. * represent $p < 0.05$ ANOVA two way corrected for multiple comparisons.

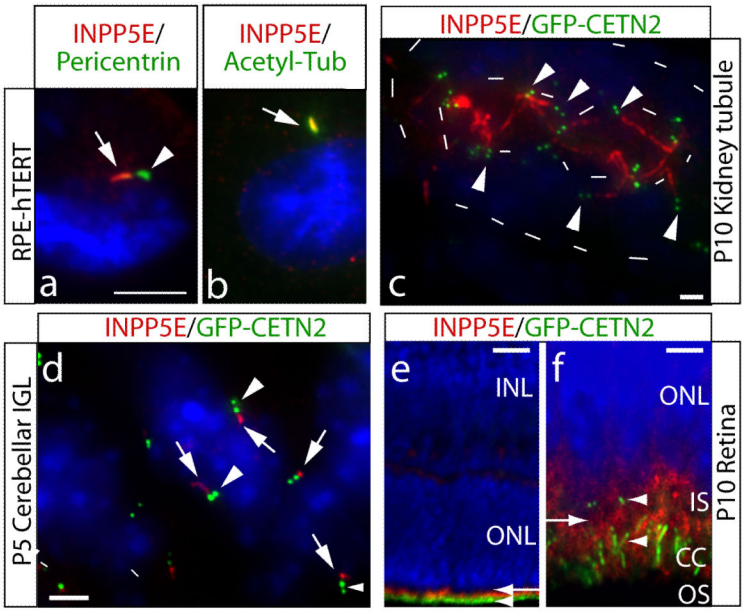

Figure 3.

Ciliary axonemal localization of INPP5E and enhanced ciliary lability in *INPP5E* mutant cell line. **(a)** RPE-hTERT ciliated cells stained for INPP5E and cilia markers. INPP5E (red, arrow) localized adjacent to pericentrin-positive (green, arrowhead) pericentriolar matrix. **(b)** Colocalization of INPP5E (red, arrow) with ciliary axonemal acetylated tubulin (green). **(c-f)** show INPP5E (red) staining in GFP-CETN2 transgenic mouse (green pair of centrioles, arrowheads). **(c)** P10 kidney collecting tubule shows INPP5E-positive red cilia projecting into the renal tubule lumen (inner dashes), limits of tubule indicated by outer dashes. **(d)** P5 cerebellar internal granule layer with INPP5E (red, arrows) ciliary axoneme adjacent to the centrioles. **(e)** P10 retina, where GFP-CETN2 labels the basal body and connecting cilium (CC, green, arrowhead). INPP5E exclusively labels photoreceptor cells (red, arrow) (**f**) High-power view of (e) showing INPP5E staining (red, arrow) in the inner segment (IS), just adjacent to and above basal bodies and CC(arrowheads). Blue = Hoechst. Scale bar 5 um (a-b,d), 25 um (c), 50 um (e), 10 um (f).

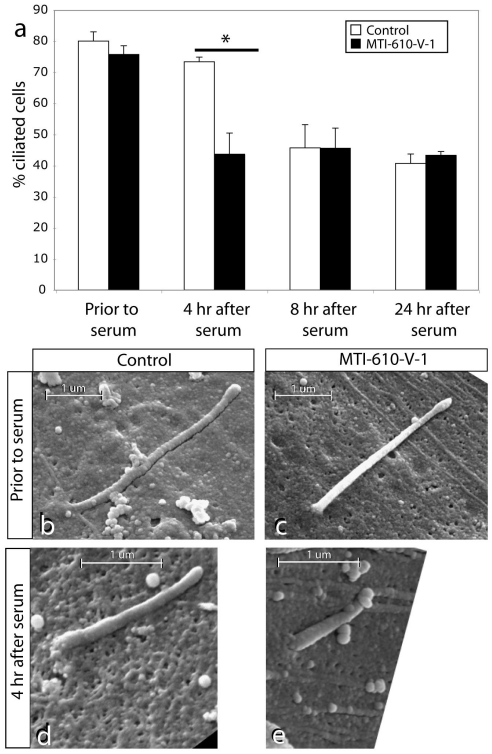

Figure 4.

(a) Lability of cilia in patient primary fibroblasts with mutant *INPP5E*. Prior to serum stimulation, serum-starved control and patient fibroblasts displayed comparable percentage of ciliated cells. By 4 hr after serum stimulation, the ciliated cells dropped to 43% in patient fibroblast as compared to 73% in control (* = $p < 0.01$, N =3, total cells counted >250 for each condition). By 8 hr or 24 hr after stimulation, ciliated cells were again comparable between patient and control samples. **(b-e)** Scanning electron micrographs of control vs. patient primary fibroblast with mutant *INPP5E*. Prior to serum stimulation, ciliary axonemal length is comparable, although slightly shorter in patient sample. By 4 hr after stimulation, axonemal length is shorter in patient sample. Scale bar indicated in um.